



# Synthesis of cationic bacterial cellulose using a templated metal phenolic network for antibacterial applications

Shuo Tang · Kai Chi · Qiang Yong · Jeffrey M. Catchmark

Received: 10 February 2021 / Accepted: 3 July 2021 / Published online: 26 July 2021  
© The Author(s), under exclusive licence to Springer Nature B.V. 2021

**Abstract** Bacterial cellulose (BC) has been an attractive bio-based material for biomedical applications due to its biocompatibility, non-toxicity, ultra-fine nanofibril network, robust mechanical properties, and high water-holding capacity. However, native BC does not possess antimicrobial properties to prevent infection that significantly limit its biomedical applications. In the present study, we have demonstrated an easy-to-functionalize biohybrid system consisting of BC and metal-phenolic network (MPN). Specifically, plant-derived tannic acid (TA) and various metal ions were complexed and embedded into a highly intertwined BC nanofibrillar network followed by cationic

functionalization to confer antimicrobial properties. The existence of MPN was successfully observed by scanning electron microscope, Fourier transform infrared spectroscopy (FT-IR) and energy-dispersive X-ray spectroscopy. Because of the synergetic antibacterial effect of TA and quaternary ammonium salts, the cationic BC@MPN composites showed good inhibitory effects on the growth of *Escherichia coli* and *Staphylococcus aureus*. This biohybrid antimicrobial BC/MPN material may have many potential applications in the food packaging and biomedical industries.

---

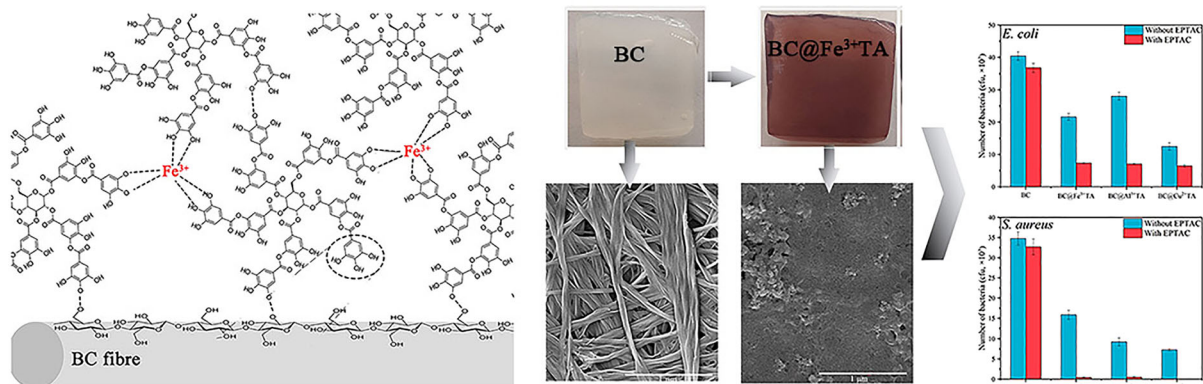
**Supplementary Information** The online version contains supplementary material available at <https://doi.org/10.1007/s10570-021-04062-8>.

---

S. Tang · Q. Yong  
Jiangsu Co-Innovation Center of Efficient Processing and Utilization of Forest Resources, College of Chemical Engineering, Nanjing Forestry University,  
Nanjing 210037, People's Republic of China

S. Tang · K. Chi · J. M. Catchmark (✉)  
Department of Agricultural and Biological Engineering,  
The Pennsylvania State University, 226 Agricultural  
Engineering Building, Shortlidge Road, University Park,  
PA 16802, USA  
e-mail: [jmc102@psu.edu](mailto:jmc102@psu.edu)

## Graphic abstract



**Keywords** Bacterial cellulose · Metal-phenolic networks · Cationization · Antibacterial

## Introduction

One of the most critical issues in wound healing is the control of infection associated with foreign microorganisms (Rahimi et al. 2020). In the past few decades, although antibiotics have become a major force in combating bacterial infections, the number of drug-resistant pathogens has increased significantly and has become a challenge for global public health (Pidcock 2012; Richter et al. 2017). As a result, researchers in related fields are working hard to develop new drugs, manufacture new materials, and explore new ways to solve the problems caused by antibiotic resistance. Gauze is widely used by doctors in the wound healing process, but it does not have antimicrobial properties (Malmsjö et al. 2009; McCallon et al. 2000). Such conditions provide a perfect environment for bacterial infections. Therefore, constructing a bandage material with antibacterial properties has become an effective method to control wound infection. Natural carbohydrate polymers having biocompatibility with human tissues and ideal physicochemical properties are widely used individually or in combination with other polymers used as wound dressings materials (Boateng et al. 2008; Zhang et al. 2017). Such multi-component materials are designed to improve the antibacterial

activity of carbohydrate gel materials against pathogenic microorganisms.

Bacterial cellulose (BC) is a fibril network composed of well-arranged three-dimensional nanofibers, which are synthesized extracellularly by certain types of bacteria, such as *Gluconobacter xylinus*, *Gluconacetobacter hansenii*, and *Gluconacetobacter pasteurianus* (Lin et al. 2013a; Reiniati et al. 2017; Torres et al. 2019). Unlike plant cellulose, BC has attracted widespread attention due to its high crystallinity, high purity, high water retention, high mechanical strength, and enhanced biocompatibility (Helenius et al. 2006; Klemm et al. 2005). However, native BC lacks certain characteristics, such as antibacterial and antioxidant properties, which are needed for many applications in the fields of biomedicine. As a result, BC composite materials have been obtained using bioactive polymers, nanomaterials, and solid particles to overcome their limitations and expand their applications (Almasi et al. 2019; Lin et al. 2013b; Tang et al. 2015). For example, BC and chitosan can form a semi-interpenetrating network hydrogel with antibacterial ability under glutaraldehyde cross-linking, and the antibacterial ability depends on the chitosan content (Wahid et al. 2019b). The new carbon quantum dot (CQD) nanoparticles have also been found to have excellent antibacterial properties and can be adsorbed on the polymer surface (Abolghasemzade et al. 2021; Malmir et al. 2020). On the other hand, a large number of hydroxyl groups on the surface of BC can be functionalized by surface modification. Until recently, few studies have conferred functional groups for

antimicrobial applications by chemically modifying the hydroxyl groups on the surface of BC but rather by obtaining cationic groups by various other means (Huang et al. 2020; Wei et al. 2011). Indeed, the well-ordered, high crystalline (crystallinity = 70–85 %) supermacromolecular structure and high water-holding capacity (up to 99 %) of never-dried, native BC have significantly limited the accessibility of chemical agents to the available surface hydroxyl groups for further functionalization, as compared to wood, plant-based and regenerated cellulosic materials.

Tannic acid (TA) is a bio-based (from plant) polyphenolic compound with high antioxidant, binding and chelating, and light adsorption properties, enabling its applications in food, medicine, and chemical industries. TA has unique structural and chemical properties, which contains galloyl groups that facilitate interactions with a variety of materials via multiple reaction pathways (Cherepanov et al. 2018). Metal chelation is a salient feature of TA (like many other polyphenols), upon which it acts as a polydentate ligand for metal ion coordination. Among them, there is a recently reported class of general-purpose metal phenolic networks (MPNs) composed of polyphenols and metal ions that allow universal design of functional surfaces and particles (Dai et al. 2019; Guo et al. 2014). The structure of MPN also depends on the pH of the solution, and the mono-, bis- and tris-species were found to prevail in the pH range 1–2, 3–6 and 7–12, respectively (Krogsgaard et al. 2014). Recently, Frank et al. reported a one-step nanosize coating process using coordination complexes of natural polyphenols and Fe(III) ions that coats various interfaces (Ejima et al. 2013). Therefore, MPNs can be used as a flexible and cost-effective surface modification method for depositing multiple types of nanoscale biological interfaces on multiple substrates. Based on this, we can perform a series of modifications on the MPNs interface to obtain the required functions. For example, poly (N-isopropylacrylamide) (PNIPAAm) is connected to MPNs deposited on a gold surface by Michael-addition or Schiff-base reaction to obtain a smart antibacterial surface layer (Wang et al. 2019). Therefore, more functions can be obtained by fixing the active material by forming a phenolic metal film on many difficult-to-react surfaces. Following a similar design strategy, a series of antibacterial surfaces modified with metal phenolic acid and biocides were prepared through

different methods, making them more suitable for long-term applications.

In this research, various BC/MPN composite materials were designed and functionalized to confer antimicrobial properties. The cationic and antimicrobial surface of BC was prepared by embedding its nanofibrillar network with a complexed TA and metal ions structure, followed by immobilization of cationic chains via a nucleophilic reaction. The properties of such cationic BC/MNP composite were characterized by UV–vis spectroscopy, FTIR–ATR spectroscopy, XRD analysis, and FESEM. The antimicrobial properties of the resulting materials were examined using two model bacterial strains including Gram-negative *Escherichia coli* (*E. coli*) and Gram-positive *Staphylococcus aureus* (*S. aureus*).

## Materials and methods

### Materials

The bacterial strain *Gluconacetobacter hansenii* (*G. hansenii*) (ATCC 53,582) was obtained from the bioresource center of American Type Culture Collection. Tannic acid, copper chloride ( $\text{CuCl}_2$ ), iron chloride ( $\text{FeCl}_3$ ), aluminum chloride ( $\text{AlCl}_3$ ) and cationic agent 2,3-epoxypropyl trimethylammonium chloride (EPTAC) were purchased from Sigma-Aldrich (Saint Louis, MO, U.S.A). All other employed reagents were A.C.S. grade and used without modification.

### Production of BC pellicles

BC was biosynthesized by *G. hansenii* by statically culturing the bacteria cells in a standard Hestrin Schramm (HS) medium containing 5 g/L yeast extract, 20 g/L glucose, 5 g/L peptone, 1.15 g/L citric acid, and 2.7 g/L  $\text{Na}_2\text{HPO}_4$  as reported previously (Hestrin and Schramm 1954). Briefly, before incubation the pH of the medium was adjusted to 5.0 and was sterilized for 20 min at 121 °C. A 5 % pre-culture of *G. hansenii* was inoculated into the liquid HS-medium and incubated statically in rectangular containers (20 × 15 × 5 cm) or 48-well plates for production of native BC pellicles. After a 3-day cultivation, BC pellicles were formed at the air–medium interface, then harvested and purified in 0.1 M NaOH aqueous

solution to remove any live cells, cell debris, medium components, and proteins at 80 °C overnight followed by rinsing with ultra-pure water (Millipore Milli-Q UF Plus) until a pH of 7 was achieved. The washed and sterilized BC pellicles were stored in ultra-pure water at 4 °C for further use.

#### Preparation of BC@Metal-TA and cationic BC@Metal-TA

To prepare BC@Metal-TA, BC pellicles (1 × 1 cm) were immersed in ultrapure water followed by adding tannic acid (TA) solution under magnetic stirring. Following TA adsorption for 1 h, metal solution was added dropwise to the above mixed solution. The pH of the solution was subsequently adjusted to ~ 7.5 with 1 mol L<sup>-1</sup> NaOH under magnetic stirring. Different samples were obtained by controlling the concentrations of TA and metal ions (Tables S1 and S2). The pellicle composites were washed with water three times to remove excess TA and metal ion.

To prepare cationic BC@Metal-TA, small pieces (1 × 1 cm) of BC@Metal-TA were soaked in 0.1 M NaOH solution. Then EPTAC (200 µL) was added dropwise into the solution, and the reaction was proceeded for 6 h at 65 °C. Finally, the pellicles were washed with water three times to remove the residual chemicals. The cationic BC@Metal-TA is named as BC@Metal-TA/EPTAC.

#### Adsorption isotherms

The native BC pellicles (20 mg dry weight) were immersed in 10 mL TA solutions of different concentrations (0.01–1 mM), respectively. After 30 min of vortex mixing to adsorb TA, the absorbance at 275 nm of these solutions was measured with a Nano drop ND-1000 UV–Vis spectrophotometer (ThermoFisher, USA). Adsorbed amounts of TA (mg/g of BC) at each concentration level were calculated from a separately constructed calibration curve.

#### In vitro release of tannic acid

The amount of the released TA from the pellicles was determined by UV spectrophotometry. One BC/TA pellicle was placed in 20 mL of PBS solution (pH = 7.5). At fixed intervals, the amount of released TA was determined by measuring the absorbance at

275 nm by using a UV–Vis spectrophotometer and comparing to the standard curves.

#### Characterization

Hydrodynamic diameters of Metal-TA solution were evaluated by a dynamic light scattering (DLS) using Zetasizer Nano ZS90 instrument (Malvern Instruments, UK) equipped with a laser (633 nm). Freshly prepared Metal-TA solution was used for particle size measurement. Samples were diluted with Milli-Q water at ambient temperature to a final concentration of 100 µM. For each sample, three DLS measurements were conducted, totaling at least 12 runs.

A UV–Vis spectrophotometer (UV-1800 spectrophotometer, Shimadzu, Japan) with 1 cm width quartz cuvettes was used to measure the absorbance of Metal-TA solutions across the range of 200–800 nm, and measurements were made at room temperature.

Fourier-transform infrared spectra (FT–IR) were recorded over the wavenumber range of 4000–400 cm<sup>-1</sup>, using a VERTEX 70 V (Bruker, Germany) spectrometer with an attenuated total reflection (ATR) diamond sensor.

The surface morphology and the structure of BC, BC@Metal-TA and BC@Metal-TA/EPTAC pellicles were characterized by field emission scanning electron microscopy (FE-SEM) equipped with energy-dispersive X-ray (EDX) spectroscopy (Nova NanoSEM, USA) with an accelerating potential of 5.0 kV, respectively. To improve surface conductivity, all the freeze-dried samples were sputter-coated with a thin layer of iridium for 30 s.

The crystallinity of BC, BC@Metal-TA and BC@Metal-TA/EPTAC pellicles was assessed by collecting X-ray diffraction diagrams using a PANalytical Empyrean diffractometer (Almelo, the Netherlands) with Cu K $\alpha$  radiation generated at 45 kV and 40 mA. The lyophilized samples were pressed into flat pieces and mounted onto a quartz sampler holder. The data were recorded in reflection mode at a rate of 2 min<sup>-1</sup> from 5°–80° with a step size of 0.026°.

#### Evaluation of antibacterial properties

The antibacterial performance of the prepared nanocomposites was assessed using *Escherichia coli* (ATCC 25,922) and *Staphylococcus aureus* (ATCC 6528). The surface of each sample (diameter: 10 mm)

was daubed with 200  $\mu\text{L}$  of adjusted germly inoculum ( $1 \times 10^4$  cfu/mL) and incubated for 6 h. A 20 mL volume of medium was added to the vial to wash out the bacteria from the samples, assisted by use of a vortex mixer. After serial dilution, 50  $\mu\text{L}$  of the germly inoculum taken out from each tube was seeded on agar plates containing medium and incubated at 37  $^\circ\text{C}$  for 24 h. Finally, the units of colony formation in each agar plate were calculated to examine the antibacterial ability.

### Statistical analysis

All experiments were carried out at least in triplicate, and results were expressed as mean  $\pm$  SD. Statistical analysis was performed using a student's t-test and SPSS 20 software.

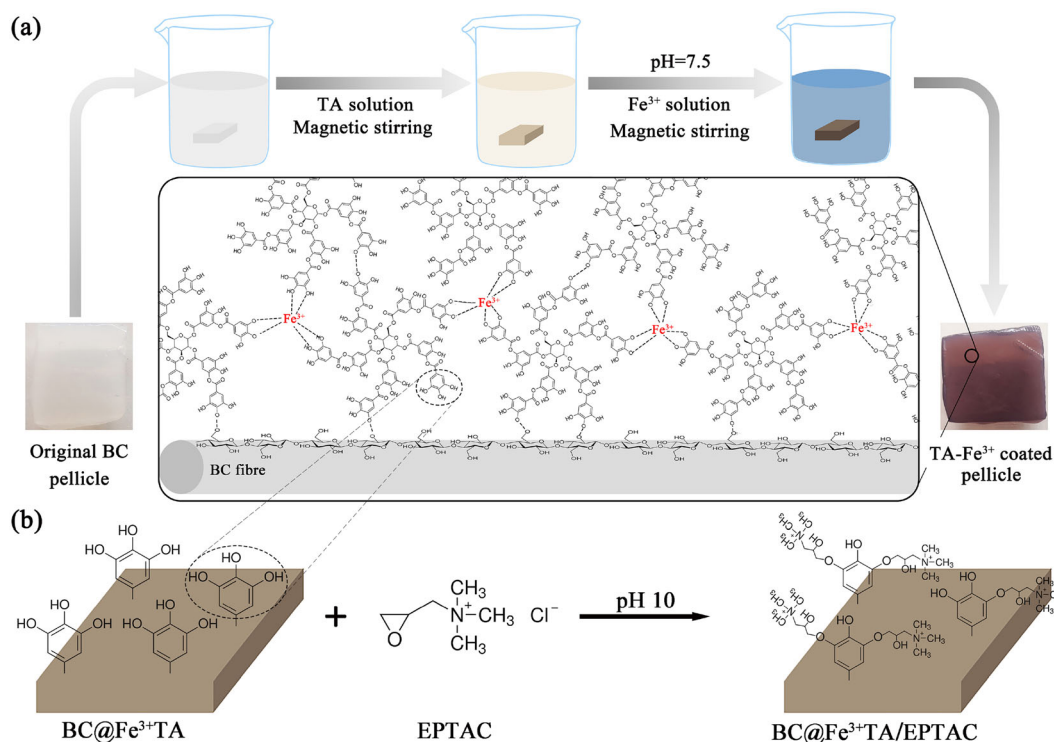
## Results and discussion

### Schematic of fabrication of BC@Metal-TA composite

Due to the polyphenolic hydroxyl structure of TA, it has a metal enabled chelation property and can interact with polydentate ligands to achieve metal ion coordination. As shown in Scheme 1, multiple TA molecules can form a network through metal ions as a cross-linking agent. TA, which contains aromatic ring structures, could interact with carbohydrates through van der Waals and hydrophobic interactions, assisted by hydrogen bonds (Limaye et al. 2019). Therefore, this metal phenolic acid network can be used for surface modification or coating of BC pellicles. This coating will simplify further modification of the material surface, such as cationization, as shown in Scheme 1.

The formation of the metal phenolic acid network is affected by the concentration of TA, the molar ratio of TA to metal ions, and pH. Figure 1 shows the effect of different ratios of TA and  $\text{Fe}^{3+}$  on the reaction. The rapid adhesion of TA on the BC pellicles was confirmed by adsorption experiments (Fig. S1). In all experiments, we controlled the pH to 7.5, because a tris-complex state was formed when the pH was greater than 7, which helped the stability of the system (Ejima et al. 2013; Krogsgaard et al. 2014). In general, iron ions precipitated completely at pH 3.2 in the

absence of TA. When TA was present, the  $\text{Fe}^{3+}$  were first stabilized to form a stable solution. With an increase of  $\text{Fe}^{3+}$  concentration, the color of the system gradually became darkened, and when the concentration was too high, it would precipitate again. Under the condition that the molar ratio of TA to  $\text{Fe}^{3+}$  was unchanged, increasing the concentration of TA did not cause precipitation, but only darkened the color of the system (Fig. S2). Further, we analyzed the hydrodynamic particle size of the formed complexes by dynamic light scattering (Fig. S3). The particle size distribution was the most uniform when the molar ratio of TA to  $\text{Fe}^{3+}$  is 1 to 2. Increasing the concentration will affect the dispersion of the system, and the particle size will increase. Excessive concentration leads to a large amount of aggregation, which ultimately affects the dispersion of the system. The coordination of  $\text{Al}^{3+}$  and  $\text{Cu}^{2+}$  with TA was also examined (Fig. S4). It was found that under the condition of pH 7.5,  $\text{Al}^{3+}$  would quickly form a precipitate, while  $\text{Cu}^{2+}$  turned brown and did not precipitate. A previous study has shown that a single organic ligand can coordinate with multiple metals (Guo et al. 2014). This coordination ability also depends on the metal ions, leading to different phenolic-metal networks. TA contains multiple benzene ring repeating units, resulting in a strong UV absorption capacity (Fig. S5). The characteristic absorption peaks of the TA solution appear at 220 nm and 280 nm, which is consistent with previous literature (Chen and Hagerman 2005). With the addition of  $\text{Fe}^{3+}$  and  $\text{Al}^{3+}$ , its characteristic absorption wavelength at 280 nm undergoes a slight red shift, indicating that a complexation reaction occurred between TA and metal ions. However, after the coating formed on the BC, the absorbance decreased, indicating that part of the TA has been adsorbed on the BC pellicles. On the other hand, the release of TA from  $\text{Fe}^{3+}$ -TA on BC pellicles was demonstrated by *in vitro* release experiments (Fig. S6). Although the sample was washed 5 times before the experiment, some TA still penetrated into the solution in the early stage. This may be due to the presence of partially free TA in the fiber network of BC pellicles. After 15 days, it stabilized. This proves the relatively stable adsorption of Fe-TA in BC pellicles. In summary, TA and metal ions were successfully coordinated and adsorbed onto the BC pellicles.



**Scheme 1** a Schematic illustration of BC pellicles coating procedure by a rapid one-step coordination assembly of tannic acid (TA) and Fe<sup>3+</sup> on a BC pellicle. b Proposed mechanism of reaction between TA (BC@Fe<sup>3+</sup>TA) and EPTAC

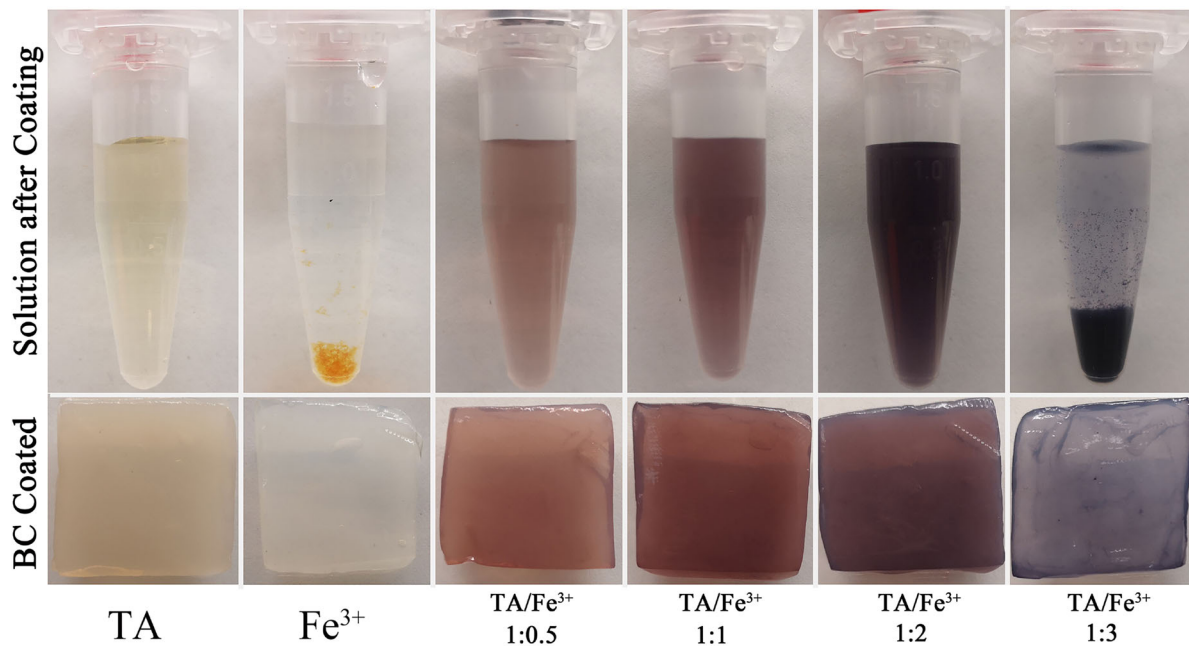


**Fig. 1** Photograph of BC pellicles and solution after different Fe<sup>3+</sup>-TA coating (TA concentration is 0.2 mM, pH = 7.5, BC pellicle size is 1 × 1 cm)

## Morphology and chemical structure characterization

ATR-FTIR spectroscopy was used to characterize BC, TA, EPTAC, BC@Metal-TA, and BC@Metal-TA/EPTAC. As shown in Fig. 2a, the BC exhibited typical cellulose vibration bands. The characteristic peaks at  $3342\text{ cm}^{-1}$  corresponded to hydroxyl groups and inter- and intramolecular hydrogen bonds and the peaks near  $2895\text{ cm}^{-1}$  were attributed to C–H stretching of  $\text{CH}_2$  and  $\text{CH}_3$  groups (Chi and Catchmark 2017). In the spectrum of TA, the characteristic broad band at  $3650\text{--}2800\text{ cm}^{-1}$  was due to stretching vibration of the phenolic ( $-\text{OH}$ ) group. Two common bands at  $1698$  and  $1604\text{ cm}^{-1}$  were coordinated to carbonyl  $\text{C}=\text{O}$  vibration of TA ester bonds and C–C stretching vibrations of aromatic rings (Ninan et al. 2016). In the  $\text{BC@Fe}^{3+}\text{TA}$  composites, the characteristic peaks of TA at  $1689$  and  $1604\text{ cm}^{-1}$ , BC at  $2895\text{ cm}^{-1}$  were also found. With the increase of TA concentration, the characteristic peaks from TA became more obvious, but the C–H characteristic peaks from BC weakened and were covered by the phenol hydroxyl peak of TA. The same result can be found at  $\text{BC@Al}^{3+}\text{TA}$  and  $\text{BC@Cu}^{2+}\text{TA}$  composites (Fig. S7). These results indicated that TA has been successfully introduced into the BC matrix.

Under alkaline conditions, cationic groups were grafted onto BC@Metal-TA through the reaction of the epoxy group of EPTAC with the phenolic hydroxyl group of TA. As shown in Fig. 2b, EPTAC has a

characteristic absorption peak at  $1478\text{ cm}^{-1}$ , corresponding to the methyl groups of ammonium (Ren et al. 2006). This characteristic peak also appeared in the cationized  $\text{BC@Metal-TA}$ . A peak appeared at about  $870\text{ cm}^{-1}$  and assigned to the addition of  $-\text{OH}$  out of plane bending, present in EPTAC chains, with the OH vibration already existing in untreated cellulose (Ladhari et al. 2007). In fact, a new peak at  $1200\text{ cm}^{-1}$  was obtained after cationization of  $\text{BC@Metal-TA}$ , due to C–O–C vibration formed by epoxy and phenolic hydroxyl groups. However, none of these peaks appeared in  $\text{BC@EPTAC}$ . These observations confirm that EPTAC was not introduced on the original BC or the grafted EPTAC moiety is negligible, but successfully grafted onto the BC with Metal-TA coating. This unsuccessful grafting of EPTAC on native BC may be due to the high crystallinity of BC and its limited surface area caused by hydrated, structured water molecules around the cellulose backbone, which makes the chemical activity of its hydroxyl groups lower than that of TA, giving rise to the difficulty of reacting with the epoxy group of EPTAC.

Scanning electron microscopy (SEM) surface morphological features of  $\text{Fe}^{3+}$ -TA coated BC prepared using the different TA concentrations are presented in Fig. 3. The native BC showed an interconnected, porous nanofibrillar network structure with random orientation of ribbons. After MPN coating, numerous aggregates of  $\text{Fe}^{3+}$ -TA complex nanoparticles were distributed between and/or within adjacent BC

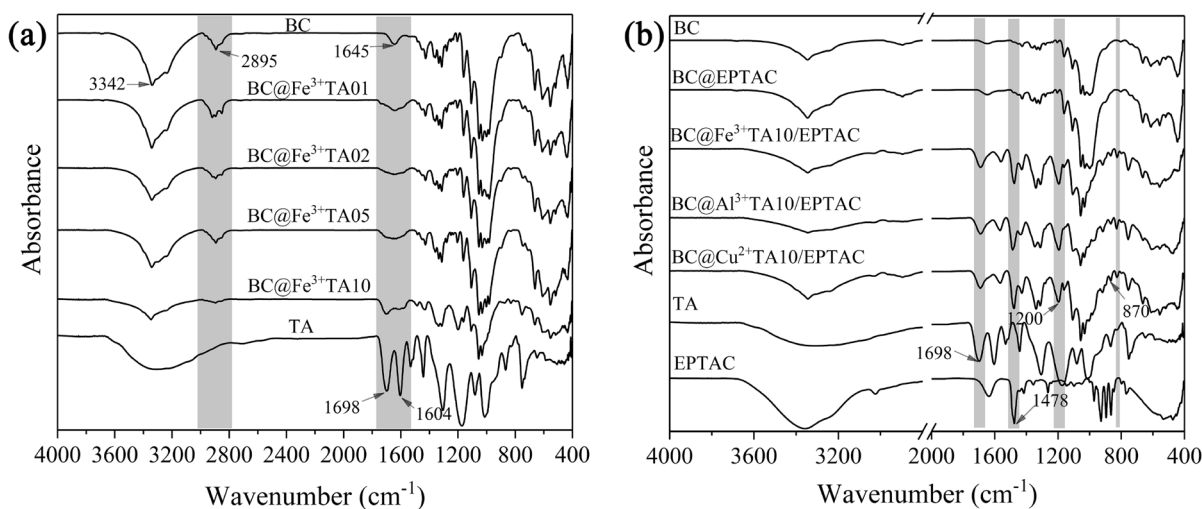


**Fig. 2** ATR-FTIR spectra of (a) pure BC, TA and  $\text{BC@Fe}^{3+}\text{TA}$ , (b) BC and  $\text{BC@Metal-TA}$  after cationization

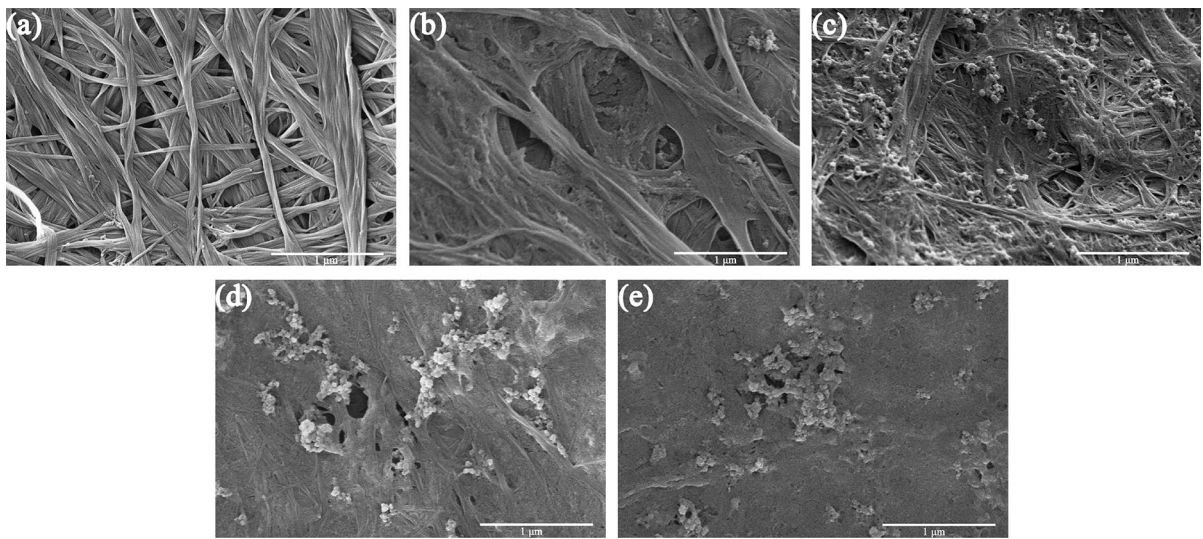


**Fig. 3** FE-SEM images of **a** pure BC, **b** BC@Fe<sup>3+</sup>TA01, **c** BC@Fe<sup>3+</sup>TA02, **d** BC@Fe<sup>3+</sup>TA05 and **e** BC@Fe<sup>3+</sup>TA10

ribbons, as well as on the surface of BC microfibril. Initially, Fe<sup>3+</sup>-TA nanoparticles were observed in the voids of the BC fiber network. When the TA concentration increased to 0.2 mM, nanoparticle spheres began to accumulate or aggregate on top of the BC network substrate. With gradual growing of concentration of TA 0.2–0.5 mM, the gaps in the intermediate layer were completely filled by Fe<sup>3+</sup>-TA nanoparticles. When the concentration further increased to 1 mM, the surface of BC ribbons was completely covered with nanoparticles, which obscured all the BC microfibrils and their network. Such similar result can be found in BC@Al<sup>3+</sup>TA and BC@Cu<sup>2+</sup>TA composite systems (Fig. S8), but differed in the degree of MPN coverage. Al<sup>3+</sup>-TA nanoparticles were more prone to stack up, while Cu<sup>2+</sup>-TA nanoparticles showed a more uniform and flattened surface. This different anchor of MPN on BC surface may be due to the different coordination assembly of metal ions with TA during the formation process, thus forming different surface stacking patterns.

The surface morphologies of different BC@Metal-TA composite cationized with EPTAC were observed using SEM (Fig. 4). Even after grafting with EPTAC, the original BC still maintained the original surface fiber morphology. Considering the FTIR results, this may again confirm that the grafting efficiency of EPTAC on BC fibril surface was negligible. After reacting with EPTAC under basic conditions, a large

number of Metal-TA nanoparticles still existed on the BC surface. However, the density of the nanoparticle spheres on the surface was relatively reduced compared to BC@MPN without cationization, possibly ascribed to the weakening of the hydrogen bonding strength at high pH conditions (Ersöz et al. 2004). Another possible reason is that the grafted EPTAC imparts a large amount of charge on the surface of the nanospheres and induces the electrostatic repulsion between the particles. These factors may have led to the shedding of some nanoparticles. In order to further reveal the effect of Metal-TA on BC, energy-dispersive X-ray (EDX) was performed to confirm the presence of metal (Fig. 4). No signature element N derived from EPTAC was found in BC@EPTAC, which indicated that EPTAC was not successfully grafted to BC or the amount was below the detection limit of EDX instrument. Elements of Fe, Al, and Cu were found in samples BC@Fe<sup>3+</sup>TA/EPTAC, BC@Al<sup>3+</sup>TA/EPTAC, and BC@Cu<sup>2+</sup>TA/EPTAC, respectively. These results fully prove successful formation of the Metal-TA network on BC substrate. At the same time, element of N appeared in all Metal-TA coated BC samples, suggesting that EPTAC was successfully grafted onto Metal-TA nanoparticles on the surface of BC.

The impact of Metal-TA coating on BC crystalline structure was studied by X-ray diffraction (XRD) (Fig. 5). XRD profile of native BC showed three main cellulose characteristic peaks at  $2\theta = 14.5^\circ$ ,  $16.7^\circ$ , and

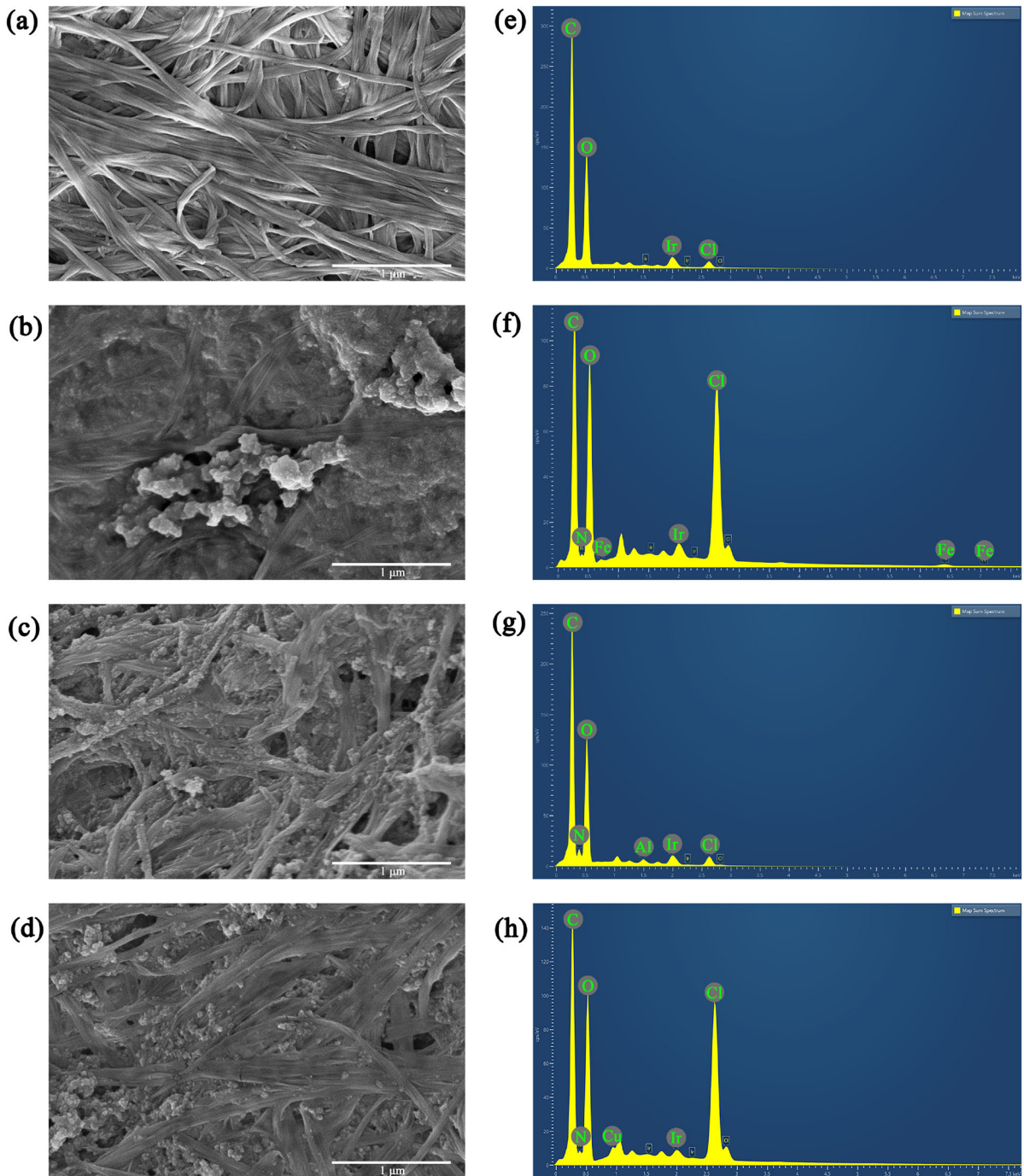


**Fig. 4** FE-SEM images of **a** BC@EPTAC, **b** BC@Fe<sup>3+</sup>TA10/EPTAC, **c** BC@Al<sup>3+</sup>TA10/EPTAC, **d** BC@Cu<sup>2+</sup>TA10/EPTAC. Energy-dispersive X-ray (EDX) spectrum of

**e** BC@EPTAC, **f** BC@Fe<sup>3+</sup>TA10/EPTAC, **g** BC@Al<sup>3+</sup>TA10/EPTAC, **h** BC@Cu<sup>2+</sup>TA10/EPTAC

22.6°, corresponding to the (100), (010), and (110) crystallographic planes, respectively (Chi and Catchmark 2017). The intensity of the peak at  $2\theta = 14.5^\circ$

was much larger than that of the peak at  $2\theta = 16.7^\circ$ , implying that cellulose produced by *G. hanseii* contained a predominant cellulose I $\alpha$  allomorph. TA

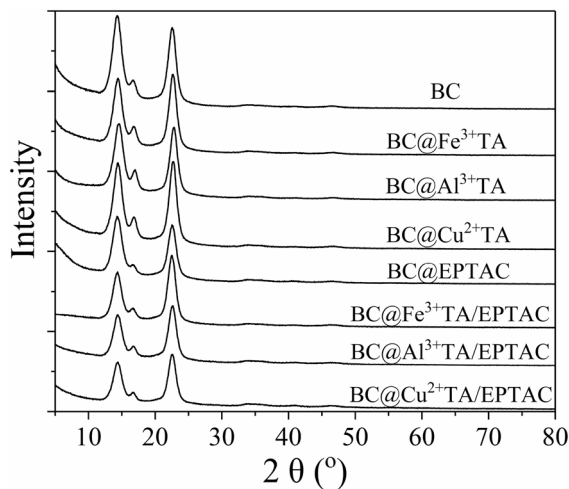


**Fig. 5** XRD curves of BC, BC@Metal-TA and BC@Metal-TA after cationization

is amorphous, showing a corresponding broad diffractogram feature instead of one or more sharp peaks as observed for crystalline structures (Chen et al. 2018). The BC@Metal-TA and cationic BC@Metal-TA show similar XRD patterns as BC, indicating that the incorporation of Metal-TA in a certain amount could maintain the crystalline structure of BC. Indeed, the biosynthesis and assembly processes of BC are hardly impacted unless interfering additives (such as xyloglucan, xylan, carboxymethyl cellulose, etc.) are incorporated in the culture medium during BC formation. Although the hydrogen bond from the phenolic hydroxyl group of the TA is stronger than the alcoholic hydroxyl group (Nose and Hojo 2006), the BC glucan chains have already formed well-ordered, hydrogen bonded crystalline structure and are therefore difficult to be affected during an ex-situ process.

### Antibacterial activity

Biomaterials with antibacterial surfaces have become urgently needed because bacterial infections are affecting millions of people worldwide. Tannic acid and quaternary ammonium salts exhibit antimicrobial activity against a broad range of bacteria (Colak et al. 2010; Saini et al. 2016). The antibacterial activity of BC@Metal-TA and cationic BC@Metal-TA composites against *E. coli* and *S. aureus* were investigated and compared (Fig. 6). For pure BC membranes used as a control, both *E. coli* and *S. aureus* grew well.

However, no significant bacterial inhibition was observed for direct cationization on pure BC. This result is completely consistent with the results of ATR-FTIR and EDX, confirming the grafting efficiency of EPTAC onto native BC fibers. Depending on the degree of the antibacterial activity of TA itself, all BC@Metal-TA composites exhibited inhibitory activities against selected bacteria strains. BC coated with only Metal-TA had a better inhibitory effect on *E. coli* than *S. aureus*. The inhibition rates of BC@Fe<sup>3+</sup>TA, BC@Al<sup>3+</sup>TA and BC@Cu<sup>2+</sup>TA on *E. coli* and *S. aureus* were 46.36 and 54.27 %, 28.96 and 73.37 %, 69.96 and 79.09 %, respectively. Previous studies have shown that TA is more resistant to *S. aureus* than *E. coli* (Mailoa et al. 2014; Widsten et al. 2010). In the same strain, the Metal-TA network formed by copper ions had higher antibacterial properties. Copper ions can damage cell walls, causing oxidative damage of proteins and inhibiting some enzymes (Baldrian 2010; Dan et al. 2005). These results cause the bacteria to be unable to divide normally and inactivate the growth of bacteria. In order to improve the antibacterial properties of the material surface, BC@Metal-TA was further cationized to form a bifunctional antibacterial surface. The results showed that the grafted cationic quaternary ammonium groups further inhibited the growth of bacteria. The inhibition rates of BC@Fe<sup>3+</sup>TA/EPTAC, BC@Al<sup>3+</sup>TA/EPTAC and BC@Cu<sup>2+</sup>TA/EPTAC on *E. coli* and *S. aureus* reached 80.07 and 98.72 %, 80.83 and 98.47 %, 82.43 and 99.93 %, respectively. It is well known that the surface of bacterial cells is negatively charged, while the quaternary ammonium groups are positively charged. As a result, electrostatic interactions caused by different charges between quaternary ammonium group and bacteria can damage cell membranes and inactivate the growth of bacteria (Murugan et al. 2010). On cationized surfaces, *S. aureus* is much less viable than *E. coli*. Quaternary ammonium compounds have less inhibitory effect on Gram negative bacteria than on Gram positive bacteria, due to the presence of lipoproteins and liposaccharides on the outer layer of peptidoglycan which hinder the attraction between antimicrobial agents (Maris 1995). Therefore, it can be concluded that Metal-TA network and quaternary ammonium cations form a synergetic antibacterial surface, of which the Metal-TA network is very important. It not only has some antibacterial effects, but also serves as a bridge between quaternary

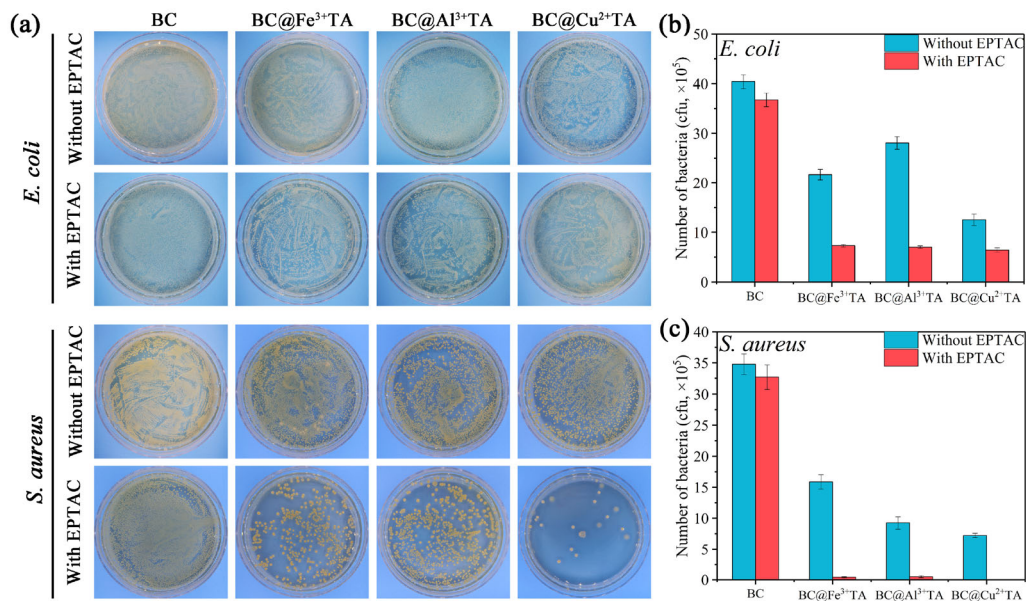


**Fig. 6** Antibacterial properties of the different samples against *E. coli* and *S. aureus*. **a** Representative photographs of bacteria (*E. coli* or *S. aureus*) colonies formed on agar plates after being

detached from different sample surfaces, **b** number of live *E. coli* detached from different sample surfaces, **c** number of live *S. aureus* detached from different sample surfaces

ammonium and BC. Similarly, this bridge can be applied to the surface of more inactive materials to obtain new materials with diverse functions.

Because of its excellent mechanical strength and reproducibility, BC has been used as a template to produce antibacterial composite materials. Table 1 summarizes the antibacterial properties of some BC compounds reported in the literature. It shows that various BC composites have different levels of antibacterial activity depending on the modification method and the nature of grafted polymers. Previous studies mainly used polymers or metals and metal oxides with antibacterial activity as filler materials. The results of this paper show that phenolic compounds as bridging grafted cationic compounds also have good effects in BC antibacterial materials and should be antibacterial candidates for many applications in daily life.

## Conclusions

In the current study, a series of metal-phenolic networks (MPN) were embedded into the ultrafine,

supermacromolecular bacterial cellulose template and further cationically functionalized to make novel cationic BC@MPN composite materials. Direct cationization of native BC was difficult, as confirmed by FT-IR, EDX, and antimicrobial results, possibly due to extremely limited accessibility of surface hydroxyl groups. In addition, the crystalline structure of BC was maintained after MPN coating and cationic functionalization. TA can be used as a bridge between quaternary ammonium salt and BC to obtain cationized BC. Antibacterial experiments showed that the bifunctional surface has a significant inhibitory effect on both *E. coli* and *S. aureus*. In particular, the modified surface can kill > 98 % of *S. aureus*. Therefore, this work can provide an efficient and widely applicable method for preparing antibacterial surfaces and is particularly suitable for the modification of inactive surfaces to obtain new functions. Simultaneously, in view of TA's excellent antioxidant function, it is also very promising in food anti-spoilage packaging.

**Authors' contributions** ST and KC contributed equally to this work. The manuscript was written through contributions of all authors. All authors have given approval to the final version of the manuscript.

**Table 1** Comparison of antibacterial properties of different BC composite materials

Materials	Functional compound	Antibacterial activity	References
OBC/COL/CS	Collagen	<i>E. coli</i> (97.6 %)	Yuan et al. (2019)
	Chitosan	<i>S. aureus</i> (98.3 %)	
BC/PEI	Polyethyleneimine	<i>E. coli</i> (> 99 %)	Wahid et al. (2019a)
		<i>S. aureus</i> (> 99 %)	
BC/PIn	Polyindole	<i>E. coli</i> (> 97 %)	Cai et al. (2018)
BC/GO	Graphene oxide	<i>E. coli</i> (95.61 %)	Shao et al. (2015)
		<i>S. aureus</i> (65.35 %)	
BC-Cu-MMT	Montmorillonite	<i>E. coli</i> (85.01 %)	Ul-Islam et al. (2012)
	Copper	<i>S. aureus</i> (79.79 %)	
BC/Cu/ZnO	Copper	<i>E. coli</i> (98.45 %)	Wasim et al. (2020)
	Zinc oxide	<i>S. aureus</i> (98.11 %)	
BC-TA-Mg <sup>2+</sup>	Tannic acid	<i>P. aeruginosa</i> (88.87 %)	Zhang et al. (2020)
	Magnesium	<i>S. aureus</i> (80.34 %)	
BC@Cu <sup>2+</sup> TA/EPTAC	Tannic acid	<i>E. coli</i> (82.43 %)	This work
	Copper	<i>S. aureus</i> (99.93 %)	
	Quaternary ammonium		

**Funding** This work was supported by the National Key R&D Program of China (2016YFD0600803), State Key Laboratory of Pulp and Paper Engineering (201812) and the USDA National Institute of Food and Agriculture Federal Appropriations under Project PAES 4602 (1009850). The authors thank the Project of First-Class Discipline and the Doctorate Fellowship of Nanjing Forestry University for supporting the work presented in this paper.

**Data availability** Authors can confirm that all relevant data are included in the article and/or its supplementary information files.

#### Declarations

**Conflict of interest** The authors declare that they have no conflict of interest.

**Consent to participate** Informed consent for publication was obtained from all participants.

**Consent for publication** All authors have seen and approved the submission and publication of the manuscript.

#### References

- Abolghasemzade S, Pourmadadi M, Rashedi H et al (2021) PVA based nanofiber containing CQDs modified with silica NPs and silk fibroin accelerates wound healing in a rat model. *J Mater Chem B* 9:658–676
- Almasi H, Mehryar L, Ghadertaj A (2019) Characterization of CuO-bacterial cellulose nanohybrids fabricated by in-situ and ex-situ impregnation methods. *Carbohydr Polym* 222:114995
- Baldrian P (2010) Effect of heavy metals on saprotrophic soil fungi. In: *Soil heavy metals*. Springer, pp263–279
- Boateng JS, Matthews KH, Stevens HNE, Eccleston GM (2008) Wound healing dressings and drug delivery systems: a review. *J Pharm Sci* 97:2892–2923
- Cai Z, Zhu C, Xiong P, Qiu Y (2018) Preparation, characterization and antibacterial activity of biodegradable polyindole/bacterial cellulose conductive nanocomposite fiber. *Membr Mater Lett* 222:146–149
- Chen Y, Hagerman AE (2005) Reaction pH and protein affect the oxidation products of  $\beta$ -pentagalloyl glucose. *Free Radic Res* 39:117–124
- Chen Y-N, Jiao C, Zhao Y, Zhang J, Wang H (2018) Self-Assembled Polyvinyl Alcohol-Tannic Acid Hydrogels with Diverse Microstructures and Good Mechanical Properties. *ACS Omega* 3:11788–11795
- Cherepanov PV, Rahim MA, Bertleff-Zieschang N, Sayeed MA, O'Mullane AP, Moulton SE, Caruso F (2018) Electrochemical behavior and redox-dependent disassembly of gallic acid/Fe(III) metal-phenolic networks. *ACS Appl Mater Interfaces* 10:5828–5834
- Chi K, Catchmark JM (2017) The influences of added polysaccharides on the properties of bacterial crystalline nanocellulose. *Nanoscale* 9:15144–15158
- Colak SM, Yapici BM, Yapici AN (2010) Determination of antimicrobial activity of tannic acid in pickling process. *Rom Biotechnol Lett* 15:5325–5330

- Dai Q et al (2019) Advancing metal–phenolic networks for visual information storage. *ACS Appl Mater Interfaces* 11:29305–29311
- Dan ZG, Ni HW, Xu BF, Xiong J, Xiong PY (2005) Microstructure and antibacterial properties of AISI 420 stainless steel implanted by copper ions. *Thin Solid Films* 492:93–100
- Ejima H et al (2013) One-step assembly of coordination complexes for versatile film and particle. *Eng Sci* 341:154–157
- Ersöz A, Denizli A, Şener İ, Atılır A, Diltemiz S, Say R (2004) Removal of phenolic compounds with nitrophenol-imprinted polymer based on  $\pi$ – $\pi$  and hydrogen-bonding interactions. *Sep Purif Technol* 38:173–179
- Guo J et al (2014) Engineering multifunctional capsules through the assembly of metal-phenolic networks. *Angew Chem Int Ed* 53:5546–5551
- Helenius G, Bäckdahl H, Bodin A, Nannmark U, Gatenholm P, Risberg B (2006) In vivo biocompatibility of bacterial cellulose. *J Biomed Mater Res Part A* 76A:431–438
- Hestrin S, Schramm M (1954) Synthesis of cellulose by aceto-bacter xylinum: 2 preparation of freeze-dried cells capable of polymerizing glucose to cellulose. *Biochem J* 58:345–352
- Huang X, Li B, Wang S, Yue X, Zhengguo Y, Deng X, Ma J (2020) Facile in-situ synthesis of PEI-Pt modified bacterial cellulose bio-adsorbent and its distinctly selective adsorption of anionic dyes. *Colloids Surf A* 586:124163
- Klemm D, Heublein B, Fink H-P, Bohn A (2005) Cellulose: fascinating biopolymer and sustainable raw material. *Angew Chem Int Ed* 44:3358–3393
- Krogsgaard M, Andersen A, Birkedal H (2014) Gels and threads: mussel-inspired one-pot route to advanced responsive materials. *Chem Commun* 50:13278–13281
- Ladhari N, Baouab MHV, Ben Dekhil A, Bakhrouf A, Niquette P (2007) Antibacterial activity of quaternary ammonium salt grafted cotton. *J Text Inst* 98:209–218
- Limaye MV et al (2019) Functionalization and patterning of nanocellulose films by surface-bound nanoparticles of hydrolyzable tannins and multivalent metal ions. *Nanoscale* 11:19278–19284
- Lin SP, Calvar IL, Catchmark JM, Liu JR, Demirci A, Cheng KC (2013) Biosynthesis, production and applications of bacterial cellulose. *Cellulose* 20:2191–2219
- Lin W-C, Lien C-C, Yeh H-J, Yu C-M, Hsu S-h (2013) Bacterial cellulose and bacterial cellulose-chitosan membranes for wound dressing applications. *Carbohydr Polym* 94:603–611
- Mailoa MN, Mahendradatta M, Laga A, Djide N (2014) Antimicrobial activities of tannins extract from guava leaves (*Psidium Guajava* L.) on pathogens microbial. *Int J Sci Technol Res* 3:236–241
- Malmir S, Karbalaie A, Pourmadadi M et al (2020) Antibacterial properties of a bacterial cellulose CQD-TiO<sub>2</sub> nanocomposite. *Carbohydr Polym* 234:115835
- Malmström J, Ingemansson R, Martin R, Huddleston E (2009) Wound edge microvascular blood flow: effects of negative pressure wound therapy using gauze or polyurethane foam. *Ann Plast Surg* 63:676–681
- Maris P (1995) Modes of action of disinfectants revue scientifique et technique-office. *Int des Epizoot* 14:47–47
- McCallon S, Knight C, Valiulus J, Cunningham M, McCulloch J, Farinas L (2000) Vacuum-assisted closure versus saline-moistened gauze in the healing of postoperative diabetic foot wounds. *Ostomy Wound Manag* 46:28–32
- Murugan E, Gopinath P, Shanmugayya V, Mathivanan N (2010) Antibacterial activity of novel insoluble bead-shaped polymer-supported multiquaternary ammonium salts. *J Appl Polym Sci* 117:3673–3678
- Ninan N, Forget A, Shastri VP, Voelcker NH, Blencowe A (2016) Antibacterial and anti-inflammatory pH-responsive tannic acid-carboxylated agarose composite hydrogels for wound healing. *ACS Appl Mater Interfaces* 8:28511–28521
- Nose A, Hojo M (2006) Hydrogen bonding of water–ethanol in alcoholic beverages. *J Biosci Bioeng* 102:269–280
- Piddock LJ (2012) The crisis of no new antibiotics-what is the way forward? *Lancet Infect Dis* 12:249–253
- Rahimi M et al (2020) Carbohydrate polymer-based silver nanocomposites: recent progress in the antimicrobial wound dressings. *Carbohydr Polym* 231:115696
- Reiniati I, Hrymak AN, Margaritis A (2017) Recent developments in the production and applications of bacterial cellulose fibers and nanocrystals. *Crit Rev Biotechnol* 37:510–524
- Ren JL, Sun RC, Liu CF, Chao ZY, Luo W (2006) Two-step preparation and thermal characterization of cationic 2-hydroxypropyltrimethylammonium chloride hemicellulose polymers from sugarcane bagasse. *Polym Degrad Stab* 91:2579–2587
- Richter MF, Drown BS, Riley AP, Garcia A, Shirai T, Svec RL, Hergenrother PJ (2017) Predictive compound accumulation rules yield a broad-spectrum antibiotic. *Nature* 545:299
- Saini S, Yücel Falco Ç, Belgacem MN, Bras J (2016) Surface cationized cellulose nanofibrils for the production of contact active antimicrobial surfaces. *Carbohydr Polym* 135:239–247
- Shao W, Liu H, Liu X, Wang S, Zhang R (2015) Anti-bacterial performances and biocompatibility of bacterial cellulose/graphene oxide composites. *RSC Adv* 5:4795–4803
- Tang L, Han J, Jiang Z, Chen S, Wang H (2015) Flexible conductive polypyrrole nanocomposite membranes based on bacterial cellulose with amphiphobicity. *Carbohydr Polym* 117:230–235
- Torres FG, Arroyo JJ, Troncoso OP (2019) Bacterial cellulose nanocomposites: an all-nano type of material. *Mater Sci Eng C* 98:1277–1293
- Ul-Islam M, Khan T, Khattak WA, Park JK (2012) Bacterial cellulose-MMTs nanoreinforced composite films: novel wound dressing material with antibacterial properties. *Cellulose* 20:589–596
- Wahid F et al (2019) Facile synthesis of bacterial cellulose and polyethyleneimine based hybrid hydrogels for antibacterial applications. *Cellulose* 27:369–383
- Wahid F, Hu X-H, Chu L-Q, Jia S-R, Xie Y-Y, Zhong C (2019) Development of bacterial cellulose/chitosan based semi-interpenetrating hydrogels with improved mechanical and antibacterial properties. *Int J Biol Macromol* 122:380–387
- Wang Y et al (2019) Smart, photothermally activated, antibacterial surfaces with thermally triggered bacteria-releasing properties. *ACS Appl Mater Interfaces* 12:21283–21291
- Wasim M, Khan MR, Mushtaq M, Naeem A, Han M, Wei Q (2020) Surface modification of bacterial cellulose by

- copper and zinc oxide sputter coating for UV-resistance/antistatic/antibacterial characteristics. *Coatings* 10:364
- Wei B, Yang G, Hong F (2011) Preparation and evaluation of a kind of bacterial cellulose dry films with antibacterial properties. *Carbohydr Polym* 84:533–538
- Widsten P, Heathcote C, Kandelbauer A, Guebitz G, Nyanhongo GS, Prasetyo EN, Kudanga T (2010) Enzymatic surface functionalisation of lignocellulosic materials with tannins for enhancing antibacterial properties. *Process Biochem* 45:1072–1081
- Yuan H, Chen L, Hong F (2019) A biodegradable antibacterial nanocomposite based on oxidized bacterial nanocellulose for rapid hemostasis and wound healing. *ACS Appl Mater Interfaces* 12:3382–3392
- Zhang L, Ge H, Xu M, Cao J, Dai Y (2017) Physicochemical properties, antioxidant and antibacterial activities of dialdehyde microcrystalline cellulose. *Cellulose* 24:2287–2298
- Zhang Z-Y et al (2020) A biocompatible bacterial cellulose/tannic acid composite with antibacterial and anti-biofilm activities for biomedical applications. *Mater Sci Eng C* 106:110249

**Publisher's Note** Springer Nature remains neutral with regard to jurisdictional claims in published maps and institutional affiliations.